ACS APPLIED MATERIALS & INTERFACES

Research Article

www.acsami.org

Facile Water-Assisted Synthesis of Cupric Oxide Nanourchins and Their Application as Nonenzymatic Glucose Biosensor

Shaodong Sun, Xiaozhe Zhang, Yuexia Sun, Shengchun Yang, Xiaoping Song, and Zhimao Yang*

School of Science, State Key Laboratory for Mechanical Behavior of Materials, MOE Key Laboratory for Non-Equilibrium Synthesis and Modulation of Condensed Matter, Xi'an Jiaotong University, Xi'an 710049, ShaanXi, People's Republic of China

Supporting Information

ABSTRACT: We have demonstrated an interesting approach for the one-pot synthesis of cupric oxide (CuO) nanourchins with sub-100 nm through a sequential dissolution−precipitation process in a water/ethanol system. The first stage produces a precursory crystal [$Cu_7Cl_4(OH)_{10}H_2O$] that is transformed into monoclinic CuO nanourchins during the following stage. Water is a required reactant for the morphology-controlled growth of different CuO nanostructures. When evaluated for their nonenzymatic glucose-sensing properties, these CuO nanourchins manifest higher sensitivity. Significantly, this water-dependent precursor transformation method may be widely used to effectively control the growth of other metal oxide nanostructures.

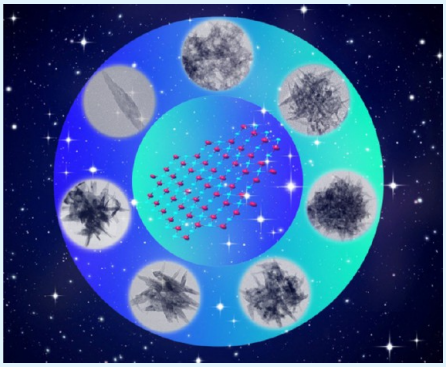

KEYWORDS: *copper oxide, nanourchins, water/ethanol, nonenzymatic glucose sensor*

1. INTRODUCTION

Metal oxide nanostructures have attracted tremendous attention because of their unique properties for many technological applications.[1] Shape and size control of metal oxide nanostructures is crucial to their sensing properties and catalytic function.[2] In addition, the multiple oxidation states of the metal components provide intriguing sensing or catalytic properties to the redox reactions.[3] Recently, Lee and co-workers have reported that electrodes made of metal oxides exhibit a remarkable electrochemical performance for the glucose biosensor.[4] Cupric oxide (CuO), as a nontoxic and low-priced material of the p-type semiconductor, exhibits great potential for wide applications in photoelectric chemical materials,[5] sensors,[6] anode materials for lithium-ion batteries,[7] supercapacitors,[8] field-emission emitters,[9] carbon monoxide oxidation,[10] and heterogeneous catalysts for olefin epoxidation.[11] So, the synthesis of new classes of CuO structures with high complexity is not only significant for a wide range of applications but also important for developing modern synthetic methodology. In the past decades, intensive attention has focused on the shape-controlled synthesis of CuO nano- and microstructures, such as nanoellipsoids,[12] nanoribbons,[13] nanorods,[14] nanotubes,[15] nanospheres,[16] nanocages,[17] microworms,[18] microflowers,[19] microurchins,[20] and nanowalnuts.[21] However, the biosensor often depends on the effective surface area and active site, making highly complex material assembly of multicomponent building blocks an excellent candidate for this application.[22,23] In this regard, aggregation of different nanosubunits into CuO hierarchical structures has been accomplished.[3,24,25] For example, Liu and Zeng performed the three-dimensional (3D) hierarchical CuO microdandelion assembly of rhombic nanoribbons by a solvent hydrothermal route in the presence of ethanol.[24] Han and co-workers fabricated 3D CuO ellipsoids composed of a hundred one-dimensional (1D) nanoparticles by a facile solution oxidative route under the assistance of formamide.[25] Song and co-workers prepared CuO hollow cubes, hollow spheres, and urchin-like particles by a dissolution−precipitation of Cu_2O cubic precursors.[3] However, these hierarchical structures always possess larger size (beyond 100 nm or microsize). In an attempt to further improve the surface area, a new category of hierarchical CuO nanocrystals with small sizes (below or around 100 nm) was imperative. To date, the relevant experimental investigation is still unavailable.

Herein, for the first time, we demonstrate the formation of polycrystalline CuO nanourchins with sub-100 nm by a one-pot solution-phase transformation of complex copper salt precursors. The single-crystalline $Cu_7Cl_4(OH)_{10}H_2O$ nanoparticles were converted to polycrystalline CuO nanourchins through a sequential dissolution−precipitation process in a water/ethanol reaction environment. Further size and shape evolution suggests that water was a required reactant for the controlled growth of hierarchical CuO nanocrystals. The synthesis of CuO nanurchins with sub-100 nm might add greater value to the nonenzymatic glucose biosensor.

Received: March 7, 2013
Accepted: April 29, 2013
Published: April 29, 2013

   dx.doi.org/10.1021/am400858j | ACS Appl. Mater. Interfaces 2013, 5, 4429−4437

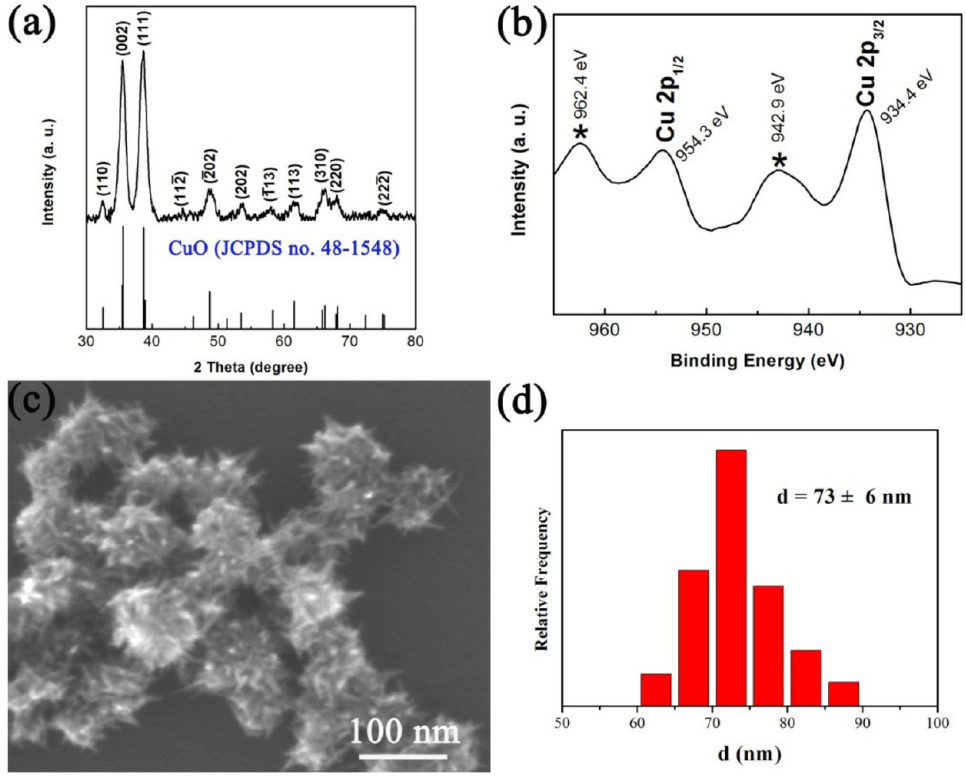

Figure 1. (a) XRD pattern of the as-prepared CuO crystals. (b) Cu 2p core-level XPS spectrum of the as-prepared CuO crystals. (c) FESEM image of the as-prepared CuO crystals. (d) Size distribution diagram of the as-prepared CuO crystals.

2. EXPERIMENTAL SECTION

2.1. Chemicals. $CuCl_2$ and sodium hydroxide (NaOH) were obtained from Aladdin Reagents. All chemicals used in our experiment were of analytical grade and were used without further purification. Deionized water (18.2 MΩ·cm) from a Milli-Q Academic water purification system (Millipore Corp.) was used in all preparations.

2.2. Synthesis of CuO Nanourchins. In a typical procedure, $CuCl_2$ (0.02 g) was first dissolved in ultrapure water (2 mL) using a beaker under constant stirring for 5 min at room temperature. Then ethanol (30 mL) was added into the copper salt solution. Afterward, the above water/ethanol solution was heated to 75 °C and stirred for 2 min. A precipitate was produced when a NaOH/ethanol solution (0.02 M) was added dropwise into the above solution. As the temperature of the mixtures was enhanced up to 75 °C again, the precipitations were further stirred for 15 min. Subsequently, the precipitations were allowed to cool to room temperature naturally. Finally, the obtained products were centrifuged at 10000 rpm for 2 min (XIANYI TG16-WS centrifuge) twice more in anhydrous ethanol and ultrapure water, respectively.

2.3. Characterization. The morphology of the powders was investigated by field-emission scanning electron microscopy (FESEM) using a JEOL microscope (JSM-7000F) at an accelerating voltage of 20 kV. Transmission electron microscopy (TEM) and high-resolution TEM (HRTEM) analyses as well as selected-area electron diffraction (SAED) analysis were performed on a JEOL JEM-2100 transmission electron microscope operating at an accelerating voltage of 200 kV. A sample for TEM analysis was prepared by ultrasonic dispersion for 60 s with ethanol (2 mL) in a 3 mL centrifuge tube. Then, the products were dropped onto a carbon-coated copper grid and dried in air before TEM analysis. Powder X-ray diffraction (XRD) patterns were recorded on a Bruker-AXS D8 ADVANCE diffractometer operated at 40 kV voltage and 40 mA current using Cu Kα radiation (λ = 1.5406 Å) in the range 20−80°. Surface analysis for the as-prepared products was performed by an X-ray photoelectron spectroscopy (XPS) using an Al Kα X-ray source operated at 90 W (England, Kratos Axis Ultra DLD).

2.4. Preparation of a CuO/Nafion/Glassy Carbon Modified Electrode and Electrochemical Measurements. An enzyme-free amperometric electrochemical sensor was prepared by casting Nafion-impregnated CuO powders onto a glassy carbon electrode (GCE) at room temperature. The modified electrode was prepared as follows: 2 mg of the final CuO powders was dispersed in a 2 mL Nafion solution (0.05%, Sigma-Aldrich). A total of 20 μL of the suspension with dispersed CuO was dropped onto the pretreated GCE (denoted as CuO/Nafion/GCE) and dried at room temperature. Before modification, the bare GCE of 5.0 mm diameter was polished to a mirrorlike surface with 0.5 μm, 0.05 μm, and 50 nm alumina slurry and then washed ultrasonically in deionized water, a 50% (v/v) nitric acid solution, ethanol, and deionized water for a few minutes, respectively. Electrochemical measurements were carried out on an Ametek VMC-4 electrochemical analyzer with a conventional three-electrode system in a 0.1 M potassium hydroxide (KOH) aqueous solution. The as-prepared CuO/Nafion/GCE was used as the working electrode with platinum foil as the counter electrode and Ag/AgCl as the reference electrode.

3. RESULTS AND DISCUSSION

3.1. Naonurchin Growth. In a typical synthesis, the copper precursor $Cu_7Cl_4(OH)_{10}H_2O$ was prepared by $CuCl_2$ and NaOH in a water/ethanol system at 75 °C. Along with an increase of the reaction time, the transformation from $Cu_7Cl_4(OH)_{10}H_2O$ to $Cu_2Cl(OH)_3$ and finally to CuO was performed through a dissolution−precipitation mechanism. The $Cu_7Cl_4(OH)_{10}H_2O$ precursors synthesized in different amounts of water/ethanol conditions would affect the competition between thermodynamics and kinetics during the transformation of precursors and nucleation and growth of CuO crystals. Significantly, water acts as both a solvent and a reactant, and it can determine the transformation of precursors into the CuO crystals.

A powder XRD pattern of the as-prepared CuO products shows a typical diffraction pattern of cuprite (JCPDS no. 48-1548), and no peaks of impurities such as $Cu_7Cl_4(OH)_{10}H_2O$, $Cu_2Cl(OH)_3$, $Cu(OH)_2$, or $CuCl_2$ were found (Figure 1a), suggesting the high purity of the as-obtained products. Further evidence for the composition and purity of the products is performed by XPS, and the core-level Cu 2p high-resolution XPS spectrum of the as-prepared products is shown in Figure 1b. The peaks correspond to the core-level Cu $2p_{1/2}$ and Cu $2p_{3/2}$ transitions of copper at 954.3 and 934.4 eV for the Cu 2p spectrum, respectively.[14] Furthermore, the presence of satellites (asterisks) on the higher binding energy sides is comparable to the values reported for the Cu 2p levels in CuO, so it can be further demonstrated that the as-prepared products are pure CuO crystals.[19] A typical FESEM image of the as-prepared CuO crystals reveals that the resulting nanostructures are well-defined nanourchins and composed of a many nanoneedles building block (Figure 1c). Statistical analysis of the FESEM data (about 80 particles) indicates that the nanosized dimensions of these nanourchins is uniform, with an average size of 73 ± 6 nm (Figure 1d).

A low-magnification TEM image of the as-prepared CuO nanourchins is shown in Figure 2a. It can also be found that the

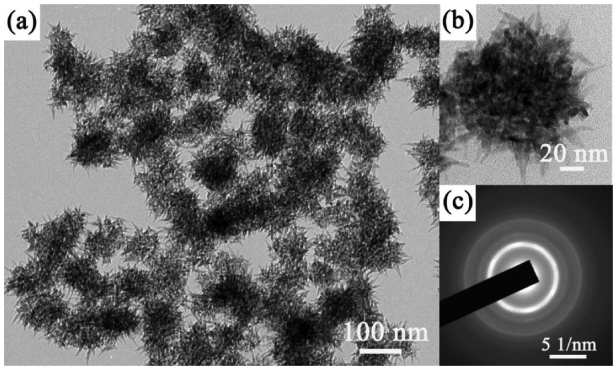

Figure 2. (a) Low-magnification TEM image of the as-prepared CuO nanourchins. (b) Typical TEM image of an individual CuO nanourchin. (c) Corresponding SAED pattern.

nanourchins are composed of a nanoneedle building block, and some of these nanoneedles have joined together and disorderly attach to form hierarchical features. Figure 2b is a typical high-magnification TEM image of an individual as-made CuO nanourchin, and it indicates that the diameter of the nanoneedle is about 6−10 nm. The corresponding SAED pattern of the individual particle is displayed in Figure 2c, suggesting that the as-prepared CuO nanourchins possess a polycrystalline nature.

HRTEM analysis of the CuO nanourchins further demonstrates that the entire nanostructure is polycrystalline. Figure 3a is a typical HRTEM image of the tip of a nanoneedle building block, and the lattice fringe of about 0.23 nm is marked by white lines and arrows, corresponding to (111) facets of monoclinic CuO crystals. Further characterization of the interior of CuO nanourchin is shown in Figure 3b, and it is clearly found that the growth directions of these (111) facets are not homogeneous and the lattice fringes of these nanoparticles have been attached (marked with the pink arrows). The inset is the corresponding fast Fourier transform image, which is expressed as a ring, suggesting the formation of a polycrystalline structure. On the basis of the aforementioned

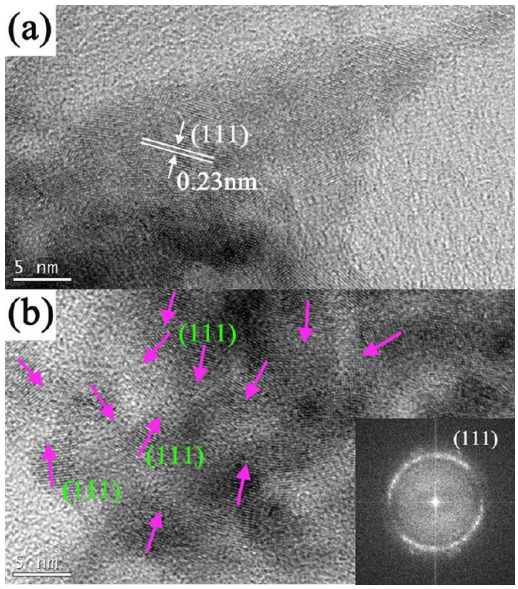

Figure 3. HRTEM image of a nanoneedle of the CuO nanourchin: (a) tip of the nanoneedle building block; (b) root of the nanoneedle building block, and the inset is the corresponding Fast Fourier transform image.

results, the branches of hierarchical CuO nanourchins (sub-100 nm) composed of a number of nanoneedles in a building block are successfully achieved.

3.2. Formation Process. Figure 4 details the structure evolution of the CuO nanourchins from different copper salt

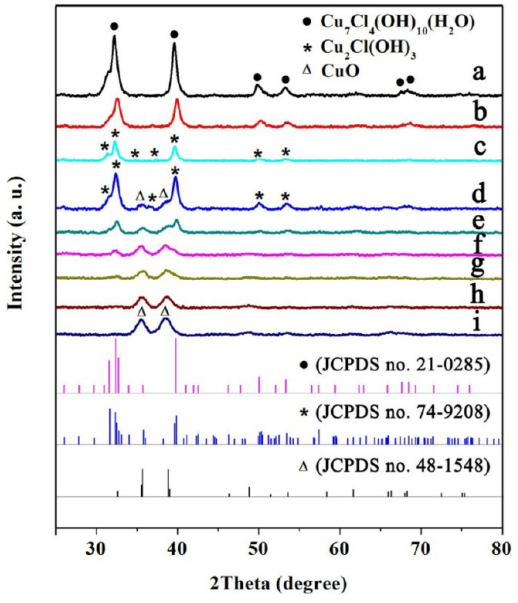

Figure 4. XRD patterns of the products obtained at different reaction stages: V_{NaOH} = (a) 6, (b) 8, (c) 10, (d) 12, (e) 20, (f) 25, (g) 30, (h) 30 (reaction time = 1 min), and (i) 30 mL (reaction time = 5 min).

precursors. The XRD pattern (Figure 4a) obtained from the product after the addition of a small amount of a NaOH solution (6 mL) was dominated by the $Cu_7Cl_4(OH)_{10}H_2O$ diffraction peaks (JCPDS no. 21-0285). No other diffractions due to crystallographic impurities such as CuO, $Cu(OH)_2$, or $CuCl_2$ were found. The XRD pattern (Figure 4b) obtained from the product after the addition of a NaOH solution (8 mL)

dx.doi.org/10.1021/am400858j | ACS Appl. Mater. Interfaces 2013, 5, 4429−4437

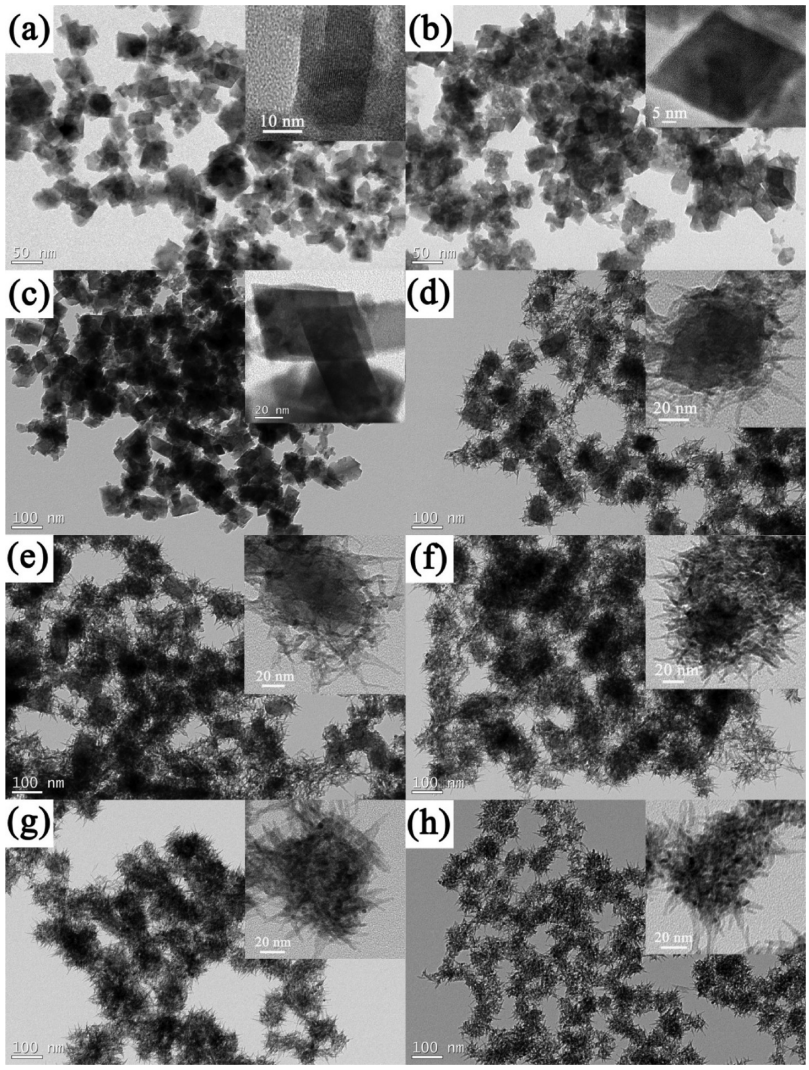

Figure 5. TEM images of the products obtained at different reaction stages: V_{NaOH} = (a) 6, (b) 8, (c) 12, (d) 20, (e) 25, (f) 30, (g) 30 (reaction time = 1 min), and (h) 30 mL (reaction time = 5 min).

exhibits an obviously weak group of diffraction peaks of $Cu_2Cl(OH)_3$, suggesting the transformation of $Cu_7Cl_4(OH)_{10}H_2O$ into intermediate $Cu_2Cl(OH)_3$ products. The XRD pattern (Figure 4c) obtained from the product after the addition of a NaOH solution (10 mL) was also dominated by the diffraction peaks of atacamite $Cu_2Cl(OH)_3$ (JCPDS no. 74-9208). Also the diffraction peaks of CuO (JCPDS no. 48-1548) appeared when the amount of NaOH was 12 mL (see Figure 4d). The XRD pattern (Figure 4e) obtained from the product after the addition of a NaOH solution (20 mL) displays an obvious diffraction peak of monoclinic CuO crystals, while the diffraction peaks belonging to the $Cu_7Cl_4(OH)_{10}H_2O$ and $Cu_2Cl(OH)_3$ crystals were significantly weakened. Upon a further increase in the amount of NaOH solution (Figure 4f, 25 mL; Figure 4g, 30 mL), it can be found that the diffraction peaks of $Cu_7Cl_4(OH)_{10}H_2O$ crystals were further weakened, while the diffraction peaks of CuO were gradually stronger. Moreover, the crystallinity was enhanced [Figure 4h (1 min) → Figure 4i (5 min) → Figure 1a (15 min)] along with the reaction time increase (heat preservation). Finally, the XRD pattern obtained from the sample as shown in Figure 1a (with 15 min of heat preservation) can be indexed to pure monoclinic CuO crystals.

These XRD data correspond perfectly to the structure evolution observed in the corresponding TEM images (see Figure 5), thus suggesting a three-stage formation process. The first-stage structural formation process (after the addition of a small amount of NaOH solution) involves the reaction between $CuCl_2$ and NaOH to form the $Cu_7Cl_4(OH)_{10}H_2O$ precursory crystals (reaction 1). The second-stage structural formation process (after the addition of more NaOH solution) starts after the $Cu_7Cl_4(OH)_{10}H_2O$ precursory crystals reach their maturity. This process involves the rapid dissolution of $Cu_7Cl_4(OH)_{10}H_2O$ precursory crystals that is accompanied by a speedy intermediate $Cu_2Cl(OH)_3$ or $Cu(OH)_2$ growth process (reactions 2 and 3). The third-stage structural formation process (after the addition of NaOH = 30 mL and an increase in the reaction time) involves the $Cu(OH)_2$ intermediate crystals being gradually transformed into CuO nanourchins (reaction 4).

$$7Cu^{2+} + 10OH^- + 4Cl^- + H_2O \rightarrow Cu_7Cl_4(OH)_{10}H_2O \quad (1)$$

$$2Cu_7Cl_4(OH)_{10}H_2O + OH^- \rightarrow 7Cu_2Cl(OH)_3 + Cl^- + H_2O \quad (2)$$

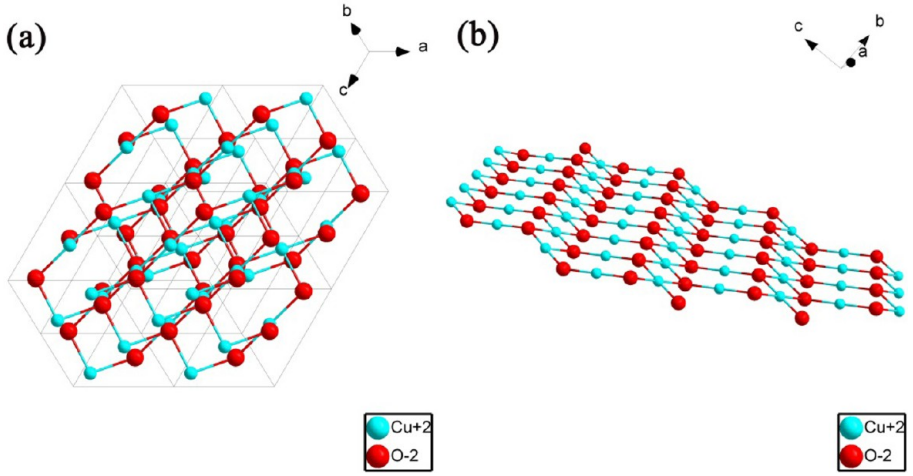

Figure 6. (a) Crystal structure of the CuO crystal. (b) Corresponding {111} facets of the CuO crystal.

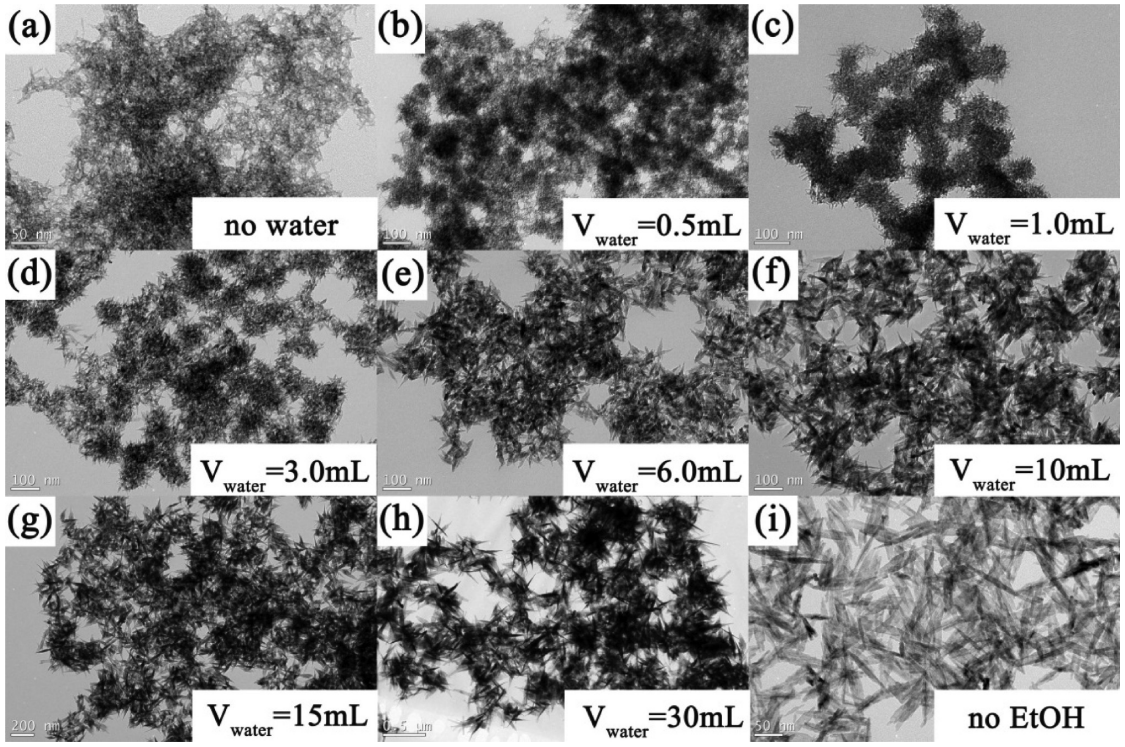

Figure 7. TEM images of different CuO nanostructures obtained in different amounts of water under otherwise similar conditions: (a) in the absence of water; V_{water} = (b) 0.5, (c) 1.0, (d) 3.0, (e) 6.0, (f) 10, (g) 15, and (h) 30 mL; (i) in the absence of ethanol.

$$Cu_2Cl(OH)_3 + H_2O \rightarrow 2Cu(OH)_2 + HCl \quad (3)$$

$$Cu(OH)_2 \rightarrow CuO + H_2O \quad (4)$$

3.3. Growth Mechanism. According to the above reaction mechanism, a sequential precursor dissolution−precipitation mechanism was given as follows. Initially, by the addition of a small amount of a NaOH solution to a $CuCl_2$ solution (under weakly acidic conditions), $Cu_7Cl_4(OH)_{10}H_2O$ (light-blue precipitate) can be formed in the presence of Cl^- ions (reaction 1). Also these $Cu_7Cl_4(OH)_{10}H_2O$ would be rapidly converted into $Cu_2Cl(OH)_3$ under an alkaline environment (reaction 2). Subsequently, $Cu_2Cl(OH)_3$ would be slowly converted into divalent $Cu(OH)_2$ in water conditions (reaction 3; see Figure 4e−g). However, $Cu(OH)_2$ is a metastable phase that is easily transformed into more stable CuO by thermal dehydration in aqueous media,[26] because the solubility of copper hydroxide is 1.3×10^{-5} mol·L^{-1}, which is higher than that of CuO (2×10^{-7} mol·L^{-1}).[27] So, the loss of water of $Cu(OH)_2$ would be generated by an oxolation process at relatively higher temperature; the hydrogen bonds that interconnect the $Cu(OH)_2$ precursors are easy to destroy, which involves a dehydration process and the formation of O−Cu−O bridges. Finally, a thermodynamically stable monoclinic CuO crystal crossing bonds of CuO_4 (Figure 6a) is prepared and precipitated to yield solid particles by decomposition of the $Cu(OH)_2$ species (reaction 4).[28] From reactions 1−4, it can be seen that the higher pH value can change the transformation process.[26] In order to further investigate the role of OH^- groups in the formation of CuO crystals, a control experiment was employed by altering the molar ratio between OH^- and

dx.doi.org/10.1021/am400858j | ACS Appl. Mater. Interfaces 2013, 5, 4429−4437

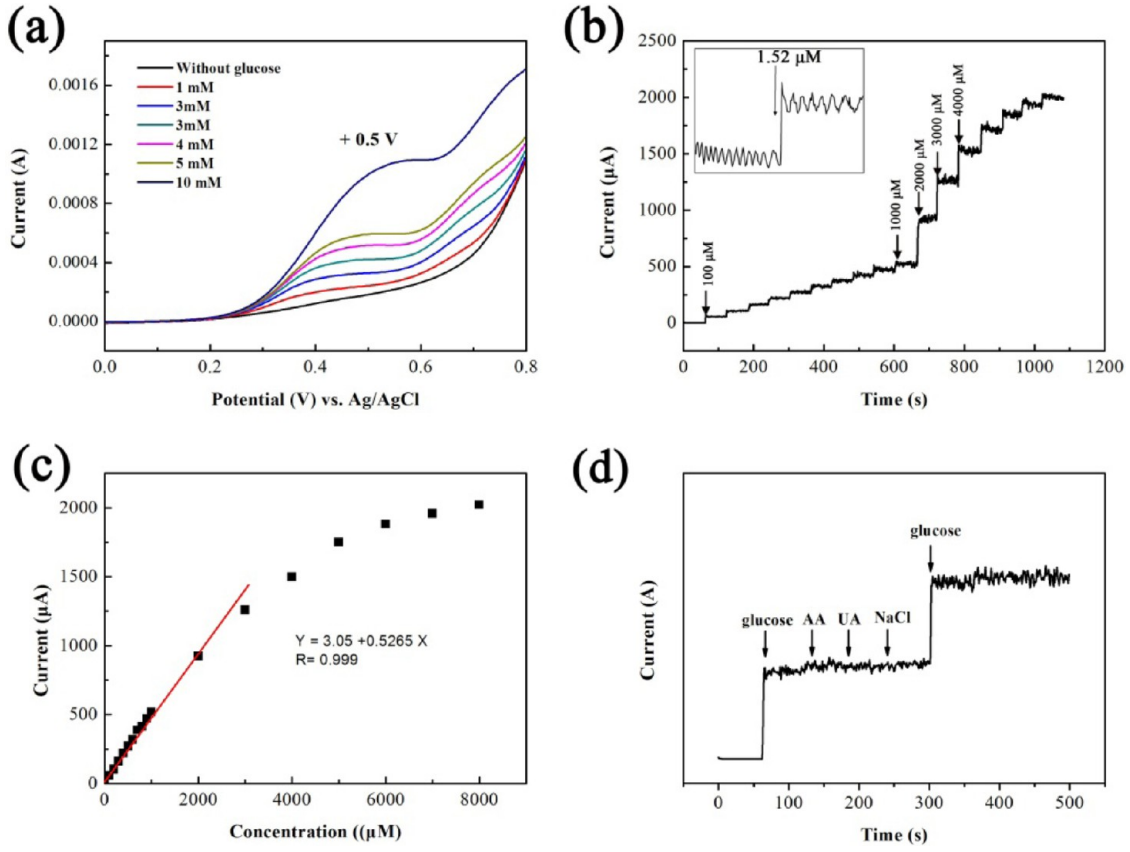

Figure 8. (a) Linear-sweep voltammograms collected for as-prepared CuO/Nafion/GCE in a range of glucose concentrations between 0 and 10 mM. (b) Amperometric response of CuO/Nafion/GCE with successive additions of different glucose amounts to 0.1 M KOH at 0.50 V vs Ag/AgCl. (c) Current−glucose concentration calibration curve obtained for the as-prepared CuO/Nafion/GCE. (d) Anti-interference property of CuO/NFs/GCE to the stepwise addition of 10 μM AA, 10 μM UA, and 10 μM NaCl, followed by the successive addition of 100 μM glucose solutions.

Cu^{2+} ions under otherwise similar conditions. The TEM images and XRD patterns of the corresponding products were displayed in Figures S1 and S2 (see the Supporting Information), respectively. It indicated that the $Cu_7Cl_4(OH)_{10}H_2O$ nanostructures were formed in a lower basic environment, while CuO nanourchins can be synthesized in an appropriate amount of NaOH. Additionally, higher reaction temperature also played an important role in the transformation of $Cu_7Cl_4(OH)_{10}H_2O$ precursors into the CuO nanourchins (Figure S3, Supporting Information).

However, the morphologies of CuO species depend on not only the precursor formation temperature and the molar ratio between NaOH and the copper salt but also the volume ratio between water and ethanol because the polarity of ethanol is less than that of water, which suggests that the electrical force between any two charges in a hydroxyl group system is much stronger.[21] Selective adsorption between the hydroxyl groups of ethanol molecules and positively charged surfaces of $Cu_7Cl_4(OH)_{10}H_2O$ can easily occur,[21] leading to the transformation of $Cu_7Cl_4(OH)_{10}H_2O$ precursors into different CuO crystals by controlling the volume ratio between water and ethanol (reactions 1−4). Furthermore, the {111} facets of CuO crystals are formed by both Cu and O atoms (see Figure 6b), and surface Cu atoms with dangling bonds on the {111} facets can make them positively charged,[29] so the {111} facets can be strongly protected by polar-charged hydroxyl groups in a high amount of ethanol, which corresponds perfectly to the structural feature observed in the HRTEM image of the as-prepared CuO nanourchins (see Figure 3). Thus, the strain energy possibly can be stored in the CuO interfaces during the mass exchange process in the formation of O−Cu−O bridges. Finally, reduction of the surface free energy by fusion and elimination of the high-activity interfaces can drive the spontaneous ordering assembly to form the hierarchical CuO nanourchins from the $Cu_7Cl_4(OH)_{10}H_2O$ precursors in the presence of a high amount of ethanol capping. However, the {111} facets of the CuO crystal would be weakly protected by hydroxyl groups in a high amount of water, so the new nanosubunits might grow up to form novel stable morphologies. Hence, it can be proposed that water is a required capping agent and reactant (reaction 3) for the shape-controlled synthesis of CuO nanostructures in the present reaction system.

3.4. Control Growth. In the present work, we have successfully converted $Cu_7Cl_4(OH)_{10}H_2O$ precursors into different CuO nanostructures by adjusting the volume ratio between water and ethanol, and more dramatic effects were observed with an increase of the water amounts (see Figure 7). Irregular netlike structures composed of many nanoneedles (see Figure 7a) were formed in the absence of water under otherwise similar conditions. The corresponding XRD pattern is shown in Figure S4a (see the Supporting Information), and the diffraction peaks belonging to the copper chlorate hydrate $Cu(ClO)_4(H_2O)_6$ crystals (JCPDS no. 13-1762) were found, so water determined the formation of $Cu_7Cl_4(OH)_{10}H_2O$ precursors. Upon the addition of a small amount of water (0.5 mL) into the ethanol solvent, some urchin-like CuO nanostructures (see Figure 7b) began to be seen (see Figure S4b, Supporting Information; JCPDS no. 48-1548). Upon

further increases in the amount of water to 1.0 and 3.0 mL, obvious CuO nanourchins were formed (see Figure 7c,d), and the diffraction peaks of the CuO crystals were increased (see Figures S4c,d, Supporting Information). However, the well-defined urchin-like CuO morphology started to alter as the amount of water was enhanced to 6.0 mL, and a sample assembled by larger nanoleaf-like structures was prepared (see Figure 7e). Similarly, uniform nanoleaf assemblies subsequently obtained by an increase of water (see Figure 7f–h) and the diffraction peaks belonging to the CuO crystals were significantly enhanced (see Figure S4f–h, Supporting Information). Interestingly, it was found that the monodisperse CuO nanoleaves (Figure 7i) were finally synthesized in the absence of ethanol (V_{water} = 30 mL), suggesting that ethanol can not only limit the size of the nanosubunits but also improve aggregation of these building blocks. High hydroxide ion concentration in the reaction mixture leads to the fast dissolution and precipitation of $Cu_2Cl(OH)_3$ as in reaction 2, and the amount of water also increases the subsequent transformation process, through reactions 3 and 4. However, $Cu(OH)_2$ is highly stable at high water amounts, by reducing the growth rate of CuO through the reverse process of reaction 4. The slow CuO growth rate results in the largest single-crystalline domains in the leaflike particles, and a typical HRTEM image (see Figure S5, Supporting Information) of the sample, as shown in Figure 7i, can further support this viewpoint. This process is similar to that occurring in the previous report.[3] On the contrary, the fast precipitation of CuO at a low amount of water maintains the original urchin-like assembly by many nanoneedles with a polycrystalline feature.

On the basis of the above results, the growth of as-prepared CuO nanourchins from $Cu_7Cl_4(OH)_{10}H_2O$ precursors could be proposed as follows: CuO seeds or clusters were generated from dissolution of the $Cu_7Cl_4(OH)_{10}H_2O$ precursors at the initial dehydration stage; in order to minimize the overall energy of the reaction system, primary nanoparticles tended to aggregate rapidly in a high amount of ethanol; as time progressed, CuO nanoneedles finally fused together to form the monoclinic CuO nanourchins (see Figure 3). However, the fusion of nanoneedles could be limited in a high amount of water, leading to the formation of monodisperse nanoleaves (see Figure 7i).

3.5. Glucose Sensor. The as-prepared CuO nanourchins were employed as glucose-sensing anode materials. We have investigated a nonenzymatic glucose sensor by deposition of the aqueous dispersion of CuO powders on a GCE surface. For the investigation of an amperometric biosensor for glucose, the CuO sample was solubilized in Nafion, a perfluorosulfonated polymer, to facilitate modification of the GC electrode surface (denoted as CuO/Nafion/GCE).[30] Linear-sweep voltammograms were measured to examine the catalytic activity of modified CuO/Nafion/GCE toward glucose oxidation in a 0.1 M KOH solution in the presence of different concentrations of glucose at a scan rate of 0.02 $V{\cdot}s^{-1}$ (Figure 8a). We have performed a control experiment by investigating the cyclic voltammetry behavior of CuO/Nafion/GCE in the absence of glucose. As expected, it is found that the current signal of CuO/Nafion/GCE toward the oxidation of glucose was weak (see the black curve). In contrast, the amperometric response will increase with enhancement of the glucose concentration at all applied potentials. The as-prepared CuO nanourchins can exhibit a remarkable catalytic current peak of about 110.2 μA in an intensity of +0.50 V.

Figure 8b shows the typical current–time response plot of as-prepared CuO/Nafion/GCE in a 0.1 M KOH solution with successive stepwise changes of the glucose concentrations. The solution was vigorously stirred to guarantee good mixing of glucose with the electrolyte, and a homogeneous glucose concentration was obtained instantly. When an aliquot of the glucose solution was added into the KOH solution with stirring, as-prepared CuO/Nafion/GCE responded instantly to the substrate and the current increased steeply to reach a stable value. The amperometric response displays a steplike enhancement in accordance with the stepwise addition of glucose. The signal noise increased with the enhancement of the glucose concentration because of the accumulation of absorbed intermediate species on the electrode surfaces.[31]

Figure 8c shows the corresponding calibration curve of the CuO glucose sensor based on the amperometric results. It shows a linear region in the range of concentrations between 100 μM and 3 mM (the range of detection from 1 to 20 mM is shown in Figure S6; see the Supporting Information). The fitting equation is I (μA) = 3.05 + 0.5265C (μM) with a correlation coefficient of 0.999. The sensitivity of the present nonenzymatic glucose sensor is 2682 $\mu A{\cdot}mM^{-1}{\cdot}cm^{-2}$. The detection limit was 1.52 μM (signal-to-noise ratio = 3). The detection limit of as-prepared CuO/Nafion/GCE is relatively low among the sensors, which is much lower than the normal blood glucose level of 4.4–6.6 mM,[32] indicating that as-prepared CuO/Nafion/GCE is suitable for the electrochemical detection of blood glucose. Note that the sensitivity of our present sensing system is higher than that of other CuO materials,[33−39] as shown in Table S1, Supporting Information. The relative standard deviation of the amperometric response to 100 μM glucose at +0.50 V is 2.28% for five successive measurements, indicating the good reproducibility of as-prepared CuO/Nafion/GCE.

For a glucose sensor, interference is another important parameter affecting its electrochemical response because easily oxidative species such as ascorbic acid (AA), uric acid (UA), and sodium chloride (NaCl) usually coexist with glucose in human blood. Herein, the electrochemical sensitivity of the above interfering species was also investigated in as-prepared CuO/Nafion/GCE. Because the normal physiological level of glucose is substantially higher than the interfering agents,[40] the anti-interference effect of the modified as-prepared CuO/Nafion/GCE was tested by successive addition of 100 μM glucose at +0.50 V vs Ag/AgCl, followed by the additions of 10 μM AA, 10 μM UA, and 10 μM NaCl in a 0.1 M KOH solution, as shown in Figure 8d. It is clearly observed that an obvious glucose response was obtained, while insignificant current responses were seen for interfering species compared to glucose addition. The observations suggest that our as-synthesized CuO nanourchin demonstrates a good specificity for glucose detection in the presence of a relatively low concentration of coexisting interfering agents (Figure 8d). However, it was found that the anti-interference effect of these products decreased upon using equimolar concentrations (1 mM) of glucose, AA, UA, and NaCl (see Figure S7, Supporting Information).

The exact mechanism for the oxidation of glucose on the CuO modified electrode in an alkaline medium is still uncertain. To date, the most accepted oxidation mechanism of glucose on the modified copper-based electrodes was suggested by Marioli and Kuwana.[41] Namely, the oxidation is generated by deprotonation of glucose and isomerization to its

enediol form, followed by adsorption onto the electrode surface and oxidation by Cu^{II} and Cu^{III}. Glucose oxidation occurred in the potential range of 0.40−0.80 V, where the oxidation wave for Cu^{II}/Cu^{III} was demonstrated.[42−45] The Cu^{III} species are proposed to act as an electron-transfer medium.[46,47] During cyclic voltammetry measurement, Cu^{II} on an CuO electrode would first be oxidized to Cu^{III} (eq I). Then the oxidative Cu^{III} could catalyze glucose oxidation to generate gluconolactone, and then gluconolactone is further oxidized to glucose acid (eq II). As is schematically shown in Figure 9, the electrochemical

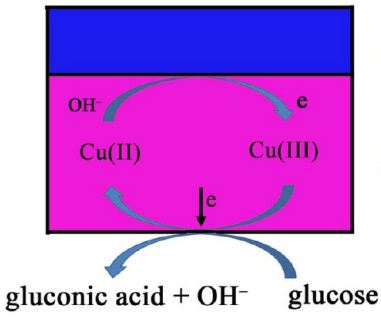

$$CuO + OH^- \rightarrow CuOOH + e \quad (I)$$

$$CuOOH + e + glucose \rightarrow CuO + OH^- + gluconic\ acid \quad (II)$$

Figure 9. Schematic of the possible pathways during nonenzymatic electrooxidation of glucose on the CuO/NFs/GCE surface in an alkaline medium.

nonenzymatic detection of glucose reduction is assisted by a Cu^{II}/Cu^{III} redox couple. Herein, the as-prepared sub-100 nm CuO nanourchins being multiple nanoparticle building blocks provide large interfaces (a high electrochemical surface) and could accelerate the diffusion of glucose molecules during kinetic electron transfer in the electrochemical process.[48]

4. CONCLUSION

In summary, we have successfully demonstrated a one-pot water/ethanol solution-phase transformation of $Cu_7Cl_4(OH)_{10}H_2O$ precursors to directly synthesize well-defined 3D nanoneedle-aggregated CuO nanourchins (sub-100 nm) through a sequential dissolution−precipitation process. Such a CuO nanourchin serving as a promising electrode material for a nonenzymatic glucose sensor shows higher sensitivity. Significantly, it is found that water is a required reactant for the formation of CuO nanostructures, and the morphology-controlled growth of monoclinic CuO nanostructures could be easily achieved by adjusting the volume ratio between water and ethanol in our reaction system. The findings reveal that different $Cu_xM_y(OH)_z$ (M = acidic radical) precursors synthesized in a water/ethanol reaction environment can be utilized to synthesize new forms of CuO nanomaterials, and this unique water-dependent precursor transformation method may be widely used to effectively control the growth of other metal oxide nanostructures.

■ ASSOCIATED CONTENT

Supporting Information

TEM images, XRD patterns, amperometric response, anti-interference property, and a comparison of the key performance characteristics. This material is available free of charge via the Internet at http://pubs.acs.org.

■ AUTHOR INFORMATION

Corresponding Author

*E-mail: zmyang@mail.xjtu.edu.cn.

Notes

The authors declare no competing financial interest.

■ ACKNOWLEDGMENTS

This work was supported by the National Science Foundation of China (Grant 51272209), Natural Science Foundation of Shaanxi Province (Grant 2011JZ008), Youth Foundation of Shaanxi Province of China (Grant 2012JQ6007), Doctoral Fund of Ministry of Education of China (Grant 20120201120051), and Fundamental Research Funds for the Central Universities.

■ REFERENCES

(1) (a) Devan, R. S.; Patil, R. A.; Lin, J. H.; Ma, Y. R. *Adv. Funct. Mater.* **2012**, *22*, 3326. (b) Wang, Z. Y.; Zhou, L.; Lou, X. W. *Adv. Mater.* **2012**, *24*, 1903. (c) Hu, J. S.; Zhong, L. S.; Song, W. G.; Wan, L. J. *Adv. Mater.* **2008**, *20*, 2977. (d) Liu, G.; Yu, J. C.; Lu, G. Q.; Cheng, H. M. *Chem. Commun.* **2011**, *47*, 6763.

(2) (a) Jun, Y. W.; Choi, J. S.; Cheon, J. W. *Angew. Chem., Int. Ed.* **2006**, *45*, 3414. (b) Liu, P.; Wang, Y.; Zhang, H. M.; An, T. C.; Yang, H. G.; Tang, Z. Y.; Cai, W. P.; Zhao, H. J. *Small* **2012**, *8*, 3664.

(3) Burda, C.; Chen, X. B.; Narayanan, R.; El-Sayed, M. A. *Chem. Rev.* **2005**, *105*, 1025.

(4) Rahman, Md. M.; Saleh Ahammad, A. J.; Jin, J. H.; Ahn, S. J.; Lee, J. J. *Sensors* **2010**, *10*, 4855.

(5) Chaudhary, Y. S.; Agrawal, A.; Shrivastav, R.; Satsangi, V. R.; Dass, D. *Int. J. Hydrogen Energy* **2004**, *29*, 131.

(6) Yang, M.; He, J.; Hu, X.; Yan, C.; Cheng, Z. *Environ. Sci. Technol.* **2011**, *45*, 6088.

(7) Zheng, S. F.; Hu, J. S.; Zhong, L. S.; Song, W. G.; Wan, L. J. *Chem. Mater.* **2008**, *20*, 3617.

(8) Wang, G. L.; Huang, J. C.; Chen, S. L.; Gao, Y. Y.; Cao, D. X. *J. Power Sources* **2011**, *196*, 5756.

(9) Hsieh, C. T.; Chen, J. M.; Lin, H. H.; Shi, H. C. *Appl. Phys. Lett.* **2003**, *83*, 3383.

(10) Qiu, G. H.; Dharmarathna, S.; Zhang, Y. S.; Opembe, N.; Huang, H. S.; Suib, S. L. *J. Phys. Chem. C* **2012**, *116*, 468.

(11) Zhu, M. Y.; Diao, G. W. *Catal. Sci. Technol.* **2012**, *2*, 82.

(12) Liu, J.; Huang, X.; Li, Y.; Sulieman, K. M.; He, X.; Sun, F. *Cryst. Growth Des.* **2006**, *6*, 16901.

(13) Wang, X. Q.; Xi, G. C.; Xiong, S. L.; Liu, Y. K.; Xi, B. J.; Yu, W. C.; Qian, Y. T. *Cryst. Growth Des.* **2007**, *7*, 930.

(14) Xiao, H. M.; Fu, S. Y.; Zhu, L. P.; Li, Y. Q.; Yang, G. *Eur. J. Inorg. Chem.* **2007**, 1966.

(15) Cao, M. H.; Hu, C. W.; Wang, Y. H.; Guo, Y. H.; Guo, C. X.; Wang, E. B. *Chem. Commun.* **2003**, 1884.

(16) Zhang, J. T.; Liu, J. F.; Peng, Q.; Wang, X.; Li, Y. *Chem. Mater.* **2006**, *18*, 867.

(17) Ng, C. H. B.; Fan, W. Y. *J. Phys. Chem. C* **2007**, *111*, 9166.

(18) Liu, X. H.; Zhang, J.; Kang, Y. F.; Wu, S. H.; Wang, S. R. *CrystEngComm* **2012**, *14*, 620.

(19) Gao, D. Q.; Yang, G. J.; Li, J. Y.; Zhang, J.; Zhang, J. L.; Xue, D. S. *J. Phys. Chem. C* **2010**, *114*, 18347.

(20) Xu, L. P.; Sithambaram, S.; Zhang, Y. S.; Chen, C. H.; Jin, L.; Joesten, R.; Suib, S. L. *Chem. Mater.* **2009**, *21*, 1253.

(21) Yu, Q.; Huang, H. W.; Chen, R.; Wang, P.; Yang, H. S.; Gao, M. X.; Peng, X. S.; Ye, Z. Z. *Nanoscale* **2012**, *4*, 2613.

(22) Park, S. H.; Kim, H. J. *J. Am. Chem. Soc.* **2004**, *126*, 14368.

(23) Aguirre, J. M.; Gutiérrez, A.; Giraldo, O.; Braz, J. *Chem. Soc.* **2011**, *22*, 546.

(24) Liu, B.; Zeng, H. C. *J. Am. Chem. Soc.* **2004**, *126*, 8124.

(25) Zhang, Z. M.; Sun, H. P.; Shao, X. Q.; Li, D. F.; Yu, H. D.; Han, M. Y. *Adv. Mater.* **2005**, *17*, 42.
(26) Sing, D. P.; Ojha, A. K.; Stivastava, O. N. *J. Phys. Chem. C* **2009**, *113*, 3409.
(27) Cudennee, Y.; Lecerf, A.; Gérault, Y. *Acad. Sci. Paris, Ser. IIc* **2000**, *3*, 661.
(28) Park, J. C.; Kim, J. H.; Kwon, H.; Song, H. *Adv. Mater.* **2009**, *21*, 803.
(29) Fei, Z. Y.; Lu, P.; Feng, X. Z.; Sun, B.; Ji, W. J. *Catal. Sci. Technol.* **2012**, *2*, 1705.
(30) Wang, J.; Musameh, M.; Lin, Y. H. *J. Am. Chem. Soc.* **2003**, *125*, 2408.
(31) Jiang, L. C.; Zhang, W. D. *Biosens. Bioelectron.* **2010**, *25*, 1402.
(32) Khatiba, K. M. E.; Hameed, R. M. A. *Biosens. Bioelectron.* **2011**, *26*, 3542.
(33) Yang, J.; Jiang, L. C.; Zhang, W. D.; Gunasekarana, S. *Talanta* **2010**, *82*, 25.
(34) Liu, S.; Tian, J. Q.; Wang, L.; Qin, X. Y.; Zhang, Y. W.; Luo, Y. L.; Asiri, A. M.; Al-Youbi, A. O.; Sun, X. P. *Catal. Sci. Technol.* **2012**, *2*, 813.
(35) Yang, Z. Y.; Feng, J. S.; Qiao, J. S.; Yan, Y. M.; Yu, Q. Y.; Sun, K. N. *Anal. Methods* **2012**, *4*, 1924.
(36) Wang, X.; Hu, C. G.; Liu, H.; Du, G. J.; He, X. S.; Xi, Y. *Sens. Actuators B* **2009**, *144*, 220.
(37) Reitz, E.; Jia, W. Z.; Gentile, M.; Wang, Y.; Lei, Y. *Electroanalysis* **2008**, *20*, 2482.
(38) Wang, W.; Zhang, L. L.; Tong, S. F.; Li, X.; Song, W. B. *Biosens. Bioelectron.* **2009**, *25*, 708.
(39) Soejima, T.; Yagyu, H.; Kimizuka, N.; Ito, S. *RSC Adv.* **2011**, *1*, 187.
(40) Li, L. M.; Du, Z. F.; Liu, S. A.; Hao, Q. Y.; Wang, Y. G.; Li, Q. H.; Wang, T. H. *Talanta* **2010**, *82*, 1637.
(41) Marioli, J. M.; Kuwana, T. *Electrochim. Acta* **1992**, *37*, 1187.
(42) Zhuang, Z. J.; Su, X. D.; Yuan, H. Y.; Sun, Q.; Xiao, D.; Choi, M. M. F. *Analyst* **2008**, *133*, 126.
(43) Luo, M. Z.; Baldwin, R. P. *J. Electroanal. Chem.* **1995**, *387*, 87.
(44) Torto, N.; Ruzgas, T.; Gorton, L. *J. Electroanal. Chem.* **1999**, *464*, 252.
(45) Wang, A. J.; Feng, J. J.; Li, Z. H.; Liao, Q. C.; Wang, Z. Z.; Chen, J. R. *CrystEngComm* **2012**, *14*, 1289.
(46) Paixao, T. R. L. C.; Corbo, D.; Bertotti, M. *Anal. Chim. Acta* **2002**, *472*, 123.
(47) Kang, X. H.; Mai, Z. B.; Zou, X. Y.; Cai, P. X.; Mo, J. Y. *Anal. Biochem.* **2007**, *363*, 143.
(48) Meher, S. K.; Rao, G. R. *Nanoscale* **2013**, *5*, 2089.